



Three-dimensional elasto-plastic analysis for the undrained capacity of ring and circular footings embedded in heterogeneous clay

Skander Hamlaoui¹ · Abdelhamid Messameh² · Abdelhak Mabrouki¹ · Imene Bougouffa¹ · Alaoua Bouaicha¹

Accepted: 10 June 2022 / Published online: 23 June 2022

© The Author(s), under exclusive licence to Springer Science+Business Media, LLC, part of Springer Nature 2022

Abstract

This paper addresses the evaluation of the bearing capacity of ring and circular footings that are embedded in non-homogeneous soils. A three-dimensional finite-difference analysis is employed using FLAC^{3D} with soil modeled as a linear elastic-perfectly plastic material following Tresca criterion. The base of the footing is attached to the soil through rough interface elements, while smooth and rough interfaces were considered along the soil-footing sides. The numerical results are validated with those available in the literature. The analyses indicated that the undrained bearing capacity factors N_c depend on the ratio of inner to outer radius (R_i/R_o), as well as the roughness of the vertical sides. In addition, the swipe loading technique is employed in order to investigate the effect of inclined and eccentric loading on the failure envelope approach. From the analyses, the failure envelopes were observed to be influenced by R_i/R_o ratio under vertical and horizontal loading. The non-dimensioned failure load in the vertical-moment V-M plane indicated that the geometry of the ring footing (R_i/R_o ratio) reduces the ultimate vertical load capacity and increases the maximum moment capacity, compared to circular footings. Hence, a negligible effect was observed for different R_i/R_o ratios in terms of normalized loads.

Keywords Ring footing · Rough side interface · Heterogeneous cohesive soil · Failure envelope

1 Introduction

Ring footings are of an economic significance; they are adopted for different structures such as silos, transmission towers, water storage tanks, and chimneys. Therefore, it is essential to understand the behavior of ring footings for a safe and

✉ Skander Hamlaoui
skander.hamlaoui@univ-biskra.dz

Extended author information available on the last page of the article

economical design. The behavior of different types of footings has been addressed by many researchers. Gourvenec et al. (2006) studied the vertical bearing capacity of square and rectangular footings resting on a homogeneous soil under undrained conditions. Mabrouki et al. (2009) used FLAC3D (2006) to calculate the bearing capacity of rigid circular footings under vertical loading for both smooth and rough soil-footing interfaces. Hence, the interference effect of strip footings has been considered by several researchers, namely, Griffiths et al. (2006), Mabrouki et al. (2010), Shu et al. (2021), and Alzabeebee (2022).

Compared to studies published on strip and circular footings, limited investigations have been made to address the behavior of ring footings. Saha (1978), Boushrehrian and Hataf (2003), Hataf and Razavi (2003), and El Sawwaf and Nazir (2012) conducted experimental analyses to compute the bearing capacity of ring foundations. Based on the method of characteristics, Kumar and Ghosh (2005) examined the behavior of cohesionless soil for different conditions pertaining to the base interface of ring footings. Using the finite difference method, Zhao and Wang (2008) considered frictional soil in order to investigate the bearing capacity factor N'_γ relevant to both smooth and rough ring footings. It was noted that the value of N'_γ is inversely proportional to the internal to external radius ratio R_i/R_0 . Thus, the factor N'_γ relevant to a rough footing base is remarkably higher than that of a smooth one.

The effect of soil heterogeneity on the bearing capacity of ring footings has been investigated by Lee et al. (2016). It was found that the undrained bearing capacity factor N_c decreases with the increase of R_i/R_0 ratio. In addition, the results showed that N_c increases in value with the raise of soil heterogeneity κ . Recently, Kedar and Deepankar (2021) addressed the effect of the footing geometry on the vertical bearing capacity of a ring foundation under undrained conditions; the thickness of the foundation was assigned to be 0.6 m in order to take into account the effect of the lateral side roughness. It was noted that the undrained bearing capacity depends on the footing geometry, such as the ratio of internal to external radius R_i/R_0 , factors of footing side roughness, embedment depths, and soil heterogeneity.

Using the failure envelope approach, Sadeghi and Bolouri (2020) performed experimental investigations to study the behavior of ring footings on frictional soil subjected to inclined and eccentric loading types. The results showed that inclined and eccentric angles dropped in value with the decrease of their corresponding vertical loads. Also, the analyses indicated that the optimal diameter ratio of ring footings is $D_i/D_0=0.4$, which results in more stability compared to other cases.

It is worth noting that the above-mentioned studies were mainly conducted for surface ring footings. Thereafter, the estimation of the bearing capacity pertaining to embedded ring footings in non-homogeneous soils with taking into account the roughness along the footing side interface did not receive much attention in the literature, neither did the effect of different loading types on the pertaining failure envelopes. The current study makes use of the finite-difference code FLAC3D (2006) in order to address the undrained bearing capacity of a rigid circular and ring footing, subjected to centric vertical loading. The influence of ratios pertaining to the internal to external radius R_i/R_0 , embedment depth D/B , and soil heterogeneity κ is considered. It should be mentioned that various interface conditions of side roughness are taken into account. Furthermore, the so called swipe loading method is

employed to study the failure envelopes in terms of both vertical-horizontal V-H and vertical-moment V-M planes, respectively, relevant to inclined and eccentric loading types.

2 Finite difference model

2.1 Geometry and material parameters

Figures 1–3 represent the problem of a rough ring footing situated on cohesive soil. For reasons of symmetry, only a quarter of the footing is considered in this part of the study. Calculations are carried out for $R_i/R_0=0, 0.25, 0.50,$ and 0.75 ; embedment ratio $D/B=0, 0.25, 0.5, 1,$ and 2 ; and footing diameter $B=2R_0=2$ m. Preliminary analyses are performed to ensure that extending the boundaries further from the footing has no effect on the calculated undrained bearing capacity. The radial and vertical boundaries are positioned away from the footing at $15R_0$ and $8R_0$, respectively. Figure 2 shows that the soil is constrained radially, and the base is fully constrained in all directions. The effect of the mesh properties on the bearing capacity was discussed earlier by Mabrouki et al. (2009); it was indicated that the bearing capacity factor is fully dependent on the pertaining mesh size and shape. Figure 3 shows that the mesh is refined gradually underneath the footing until reaching steady values of the bearing capacity; hence, the rigid footing is discretized by the finite difference zones using an elastic material with large enough shear and bulk modulus of $G=10.41$ GPa and $K=13.89$ GPa, respectively (equivalent to the Young’s modulus $E=25$ GPa and Poisson’s ratio $\nu=0.2$). The footing is attached to the soil through

Fig. 1 Undrained shear strength profile for heterogeneous soil

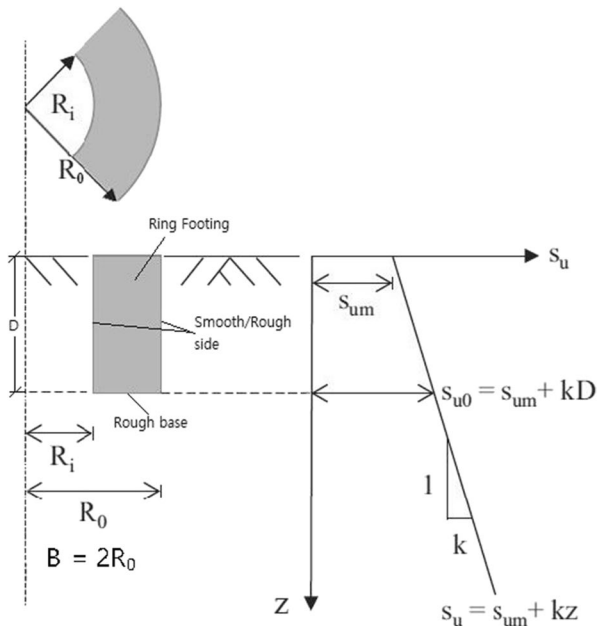


Fig. 2 Problem geometry and boundary conditions

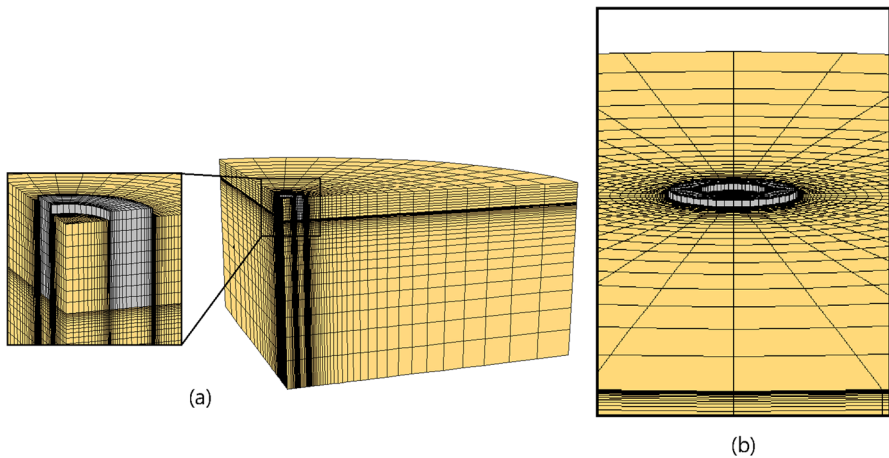
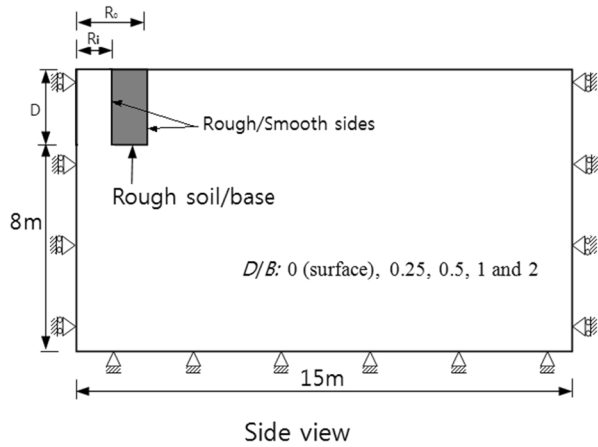


Fig. 3 Finite difference mesh: **a** quarter model, **b** full model

interface elements. The base of the footing is considered to be rough, while both smooth and rough interfaces are considered along the sides. The normal and shear stiffnesses of 105 Pa/m are assigned in the cases of rough base and side interfaces, with an interface cohesion equal to that of the soil. However, negligible shear stiffness and undrained strength are assigned in the case of a smooth side interface, with a normal stiffness of 105 Pa/m. It should be mentioned that the interface sustains zero tension; therefore, a footing detachment may be generated. The soil is modeled as a linear elastic-perfectly plastic material following the Tresca criterion, with $\varphi=0$, unit weight $\gamma=16 \text{ kN/m}^3$, and Poisson's ratio $\nu=0.49$. The linear variation of the shear strength s_u with depth is expressed as $S_u = S_{um} + kz$ (Fig. 1), where s_{um} is the shear strength at the surface, and $\kappa=kB/S_u$ is the shear strength gradient with depth z ($\kappa=0, 3, 6$ and 10). Moreover, the soil Young's modulus E_u is increasing

linearly with depth, with respect to a constant ratio of $E_u/s_u=500$, similarly to Gourvenec and Mana (2011) and Hu et al. (1999).

2.2 Finite difference computations

The software FLAC3D (2006) computes the bearing capacity relevant to circular and ring footings based on subdividing the soil into a number of zones. The finite difference zone represents the smallest geometric domain on the basis of which the change in the stress–strain plots is captured. Thusly, polyhedral zones of different shapes are employed to model the entire domain.

The ultimate load capacity q_{ult} is computed using FISH function. This is done by dividing the vertical limit load Q by the quarter of the footing area. The ultimate bearing capacity q_{ult} of the embedded ring footing is given as follows:

$$q_{ult} = \frac{4Q}{\pi(R_0^2 - R_i^2)} \quad (1)$$

where Q , R_0 , and R_i are, respectively, the ultimate vertical load including the resistance relevant to both of the footing base and vertical sides, outer and inner radiuses.

The expression of the ultimate bearing capacity pertaining to undrained clays is given also as follows:

$$q_{ult} = s_u d_c N_c S_u + q_0 = N_c^* S_u + q_0 \quad (2)$$

$$N_c^* = q_{net}/s_u \quad (3)$$

where N_c , S_u , d_c , q_0 , and N_c^* are, respectively, the bearing capacity factor, undrained shear strength, shape factor, depth factor that is defined as the ratio of the bearing capacity at depth D to that at the soil surface, surcharge ($q_0 = \gamma D$), and the net bearing capacity factor relevant to unspecified shape and embedment depth (Eq. 3), with $q_{net} = q_u - q_0$.

It is of interest to mention that the study also investigates the effect of different R_i/R_0 ratios on the load interaction curves pertaining to both V-H (inclined loading) and V-M (eccentric loading). The full model is taken into account in the simulation procedure for this part of the study, as shown in Fig. 3b. Swipe-loading technique is employed for reasons of dressing the failure envelopes. The interaction of load components pertaining to V-H loading space is given in two steps; step 1 consists of applying vertical velocities to the nodes of the footing until the ultimate vertical load (V_{ult}) is reached; thusly, a horizontal velocity is applied with preventing the footing from moving vertically until reaching the ultimate horizontal load. The second step begins directly by imposing a horizontal velocity with ignoring all vertical loads until attaining the ultimate horizontal load (H_{ult}). Moreover, the first step pertaining to the V-M load space consists of applying vertical velocities to the footing nodes until reaching the maximum ultimate vertical load V_{max} , beyond which, the moment loading is applied by assuming equal and opposite vertical velocities at the footing

Fig. 4 Load–settlement curve for surface circular footing

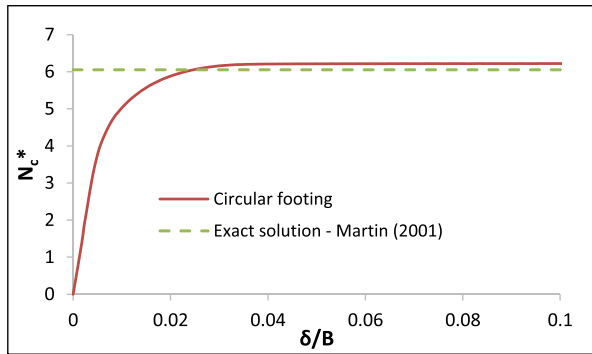
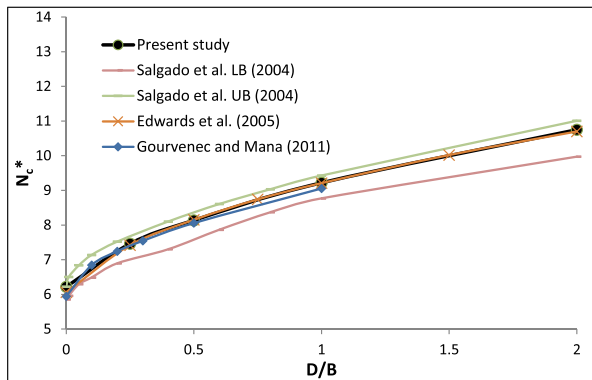


Fig. 5 Comparison of N_c for embedded circular footing in a homogeneous soil, with a smooth side interface



edges, until the ultimate moment M_{max} is reached. Hence, step 2 starts directly by applying the moment loading without taking into account the vertical loads.

3 Model verification

Computations of N_{0c} relevant to a circular shallow footing on a homogeneous soil are compared with those available in the literature. Figure 4 shows that the present study results in a factor N_{0c} pertaining to the condition of a rough base interface as high as 6.21. This latter is only 2.64% higher than the exact solution ($N_{0c}=6.05$) provided by Eason and Shield (1960), Houslyby and Wroth (1983), and Martin (2001). This result enlightens the reliability of the used finite difference analysis. Figure 5 is plotted assuming a rough base and smooth side interfaces; N_c pertaining to the case of a vertically loaded circular footing embedded in frictionless soil is computed with respect to different ranges of $D/B=0.25, 0.5, 1,$ and 2 . It should be mentioned that the bearing capacity factors pertaining to the present study are following an increasing trend with the rise of D/B ratio; hence, N_c is noticed to be within the upper and lower bounds of Salgado et al. (2004). The current plot shows an excellent agreement with that resulting from Edwards et al. (2005).

Fig. 6 Comparison of N_c relevant to the surface circular footing in a non-homogeneous soil

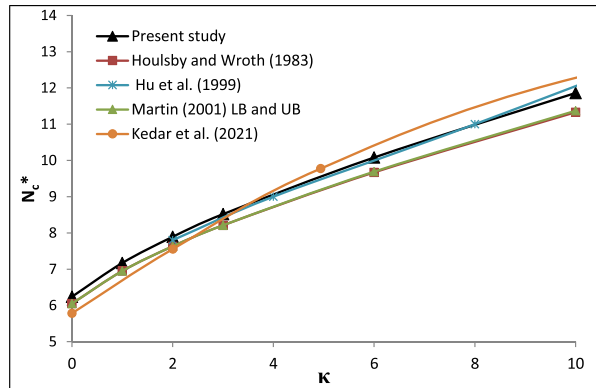


Fig. 7 Load–settlement curves for surface circular and ring footings in homogeneous soil

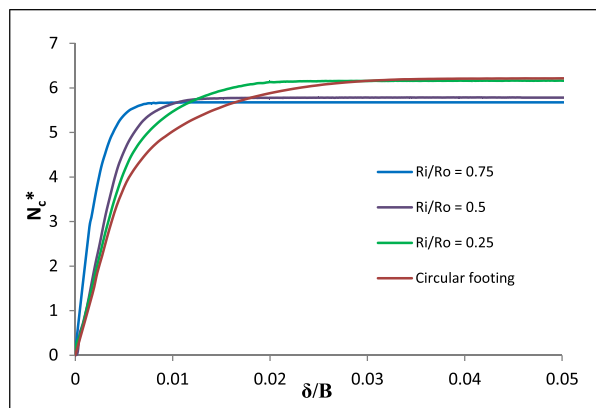


Figure 6 represents the spread out of N_c relevant to a shallow circular footing that is undergoing a central vertical loading with respect to different degrees of soil non-homogeneity κ . Using the method of characteristics, Martin (2001) gave the exact N_c factors for different κ ; hence, it was reported that for $D/B=0$ (surface circular footings), and the results pertaining to both upper and lower bound methods reach similar values. The resulting bearing capacity factor N_c increases with the raise of κ , with values that are slightly above those obtained by Martin (2001) and Gourvenec and Randolph (2003). For large κ values, N_c factors provided by Kedar and Deepankar (2021) are seen to be slightly higher than the obtained in the present study.

4 Results and discussion

The normalized load–settlement curves are plotted in Fig. 7 for surface circular and ring footings situated on a homogeneous soil; different ranges of inner to outer radius (R_i/R_o) are considered. It is noted that the applied load increases

and reaches its ultimate value at a smaller range of normalized settlement (δ/B) for high values of R_f/R_0 .

The results from the finite difference analysis are resumed in Tables 1 and 2 for both smooth and rough side interfaces, whereas the bearing capacity factor N_c is computed with respect to various ratios of R_f/R_0 , D/B , and κ . Hence, Fig. 8a shows the spread out of N_c pertaining to the case of smooth sides of the footing and homogeneous soil. It is observed that N_c is following an increasing trend until reaching an ultimate point corresponding to $R_f/R_0=0.25$, beyond which it continues dropping. Figure 8b shows that for $\kappa=10$, N_c decreases with the increase of R_f/R_0 pertaining to the surface footing. It is noticed from Fig. 8c and d that for a rough interface of the base and sides of the embedded ring footing, N_c increases as R_f/R_0 increases. This rate of increase is more prominent for a higher value of D/B ; it is interpreted by the fact that the shear strength of the sides contributes to the bearing capacity. It is worthwhile to mention that a negligible effect on the variation of N_c is revealed for

Table 1 N_c factors for ring and circular footings, smooth sides

κ	D/B	R_f/R_0			
		0.00	0.25	0.50	0.75
0	0	6.21	6.08	5.73	5.55
	0.25	7.25	7.75	7.26	7.48
	0.5	8.14	8.93	8.19	8.11
	1	9.22	10.91	9.49	9.24
	2	10.75	13.83	12.20	11.38
1	0	7.17	6.72	6.19	5.81
	0.25	8.19	8.27	7.68	7.76
	0.5	9.34	9.24	8.48	8.65
	1	10.71	10.76	9.56	9.74
	2	11.65	12.86	11.66	12.14
3	0	8.51	6.65	6.91	6.23
	0.25	8.92	8.74	8.06	8.01
	0.5	9.70	9.36	8.67	8.91
	1	10.63	10.51	9.55	9.87
	2	11.40	12.34	11.42	12.31
6	0	10.08	8.80	7.76	6.77
	0.25	9.34	9.00	8.27	8.13
	0.5	9.79	9.34	8.71	8.96
	1	10.50	10.32	9.57	10.02
	2	11.19	12.11	11.42	12.41
10	0	11.86	10.03	8.69	7.36
	0.25	9.82	9.12	8.37	8.18
	0.5	9.78	9.28	8.67	8.94
	1	10.35	10.17	9.51	10.14
	2	10.99	11.91	11.40	12.47

Table 2 N_c factors for ring and circular footings, rough sides

κ	D/B	R_f/R_0			
		0.00	0.25	0.50	0.75
0	0	6.21	6.08	5.73	5.55
	0.25	8.57	9.32	9.86	11.84
	0.5	9.48	11.57	13.33	17.25
	1	11.39	15.39	18.52	27.01
	2	14.49	21.85	26.21	42.67
1	0	7.17	6.72	6.19	5.81
	0.25	9.51	10.07	10.11	11.75
	0.5	11.05	12.06	12.86	16.03
	1	13.24	14.63	16.91	22.83
	2	16.61	18.28	22.33	33.70
3	0	8.51	7.62	6.91	6.23
	0.25	10.21	10.48	10.22	11.60
	0.5	11.19	11.93	12.30	14.94
	1	12.71	13.96	15.66	20.55
	2	15.62	17.06	20.85	30.54
6	0	10.08	8.80	7.76	6.77
	0.25	10.60	10.63	10.22	11.39
	0.5	11.16	11.73	11.89	14.28
	1	12.36	13.56	15.01	19.59
	2	15.16	16.51	20.20	29.37
10	0	11.86	10.03	8.69	7.36
	0.25	10.81	10.66	10.18	11.20
	0.5	11.11	11.60	11.63	13.94
	1	12.12	13.30	14.63	19.05
	2	14.89	16.25	19.81	28.80

the case of a surface footing in homogeneous soil; in addition, N_c continues decreasing for $\kappa=10$.

The variation of N_c in terms of R_f/R_0 with respect to different κ values is illustrated in Fig. 9. For the surface footing in Fig. 9a, N_c drops with the increase of R_f/R_0 ; this decreasing trend is more noticeable for higher values of κ . Moreover, Fig. 9c is dressed for an embedded footing with rough sides. It is clear that N_c rises with the rise of R_f/R_0 ; this is explained by the positive effect of the side shear strength on the magnitude of N_c . For the embedded footing in the heterogeneous soil with smooth sides (Fig. 9b), it is noted that there is a slight variation in N_c values to be between 11 and 13.

Figure 10 shows the variation of N_c as a function of soil heterogeneity κ . The embedment ratio D/B is varied for different roughness conditions and $R_f/R_0=0$ and 0.75. It is clear that for $\kappa>3$ in the cases of embedded footing, a negligible effect of κ is observed on the magnitude of N_c . However, this latter follows an increasing trend with the raise of κ for the case of surface footing.

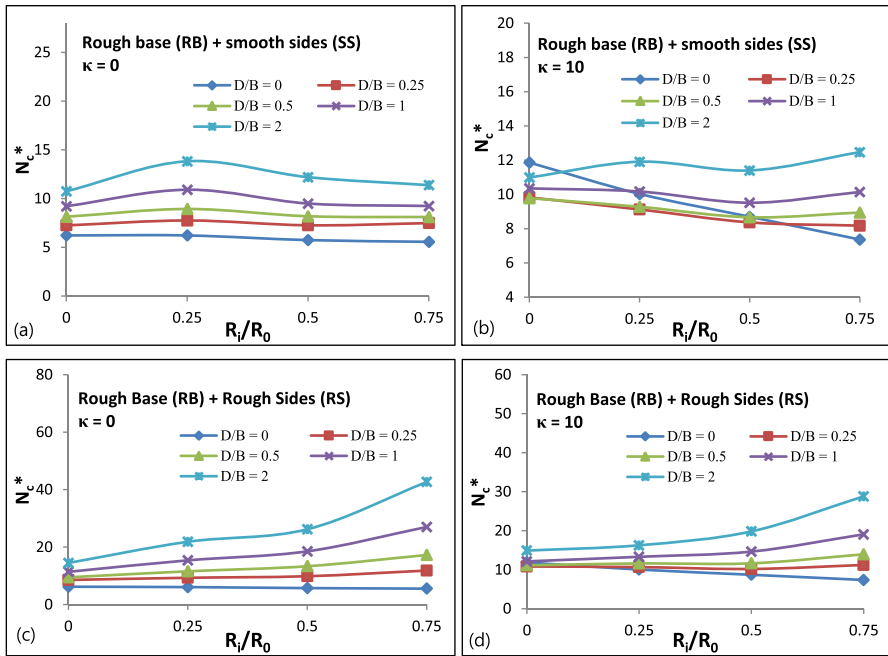


Fig. 8 N_c factor of ring footings for various embedment ratios D/B , with $\kappa=0$ and 10

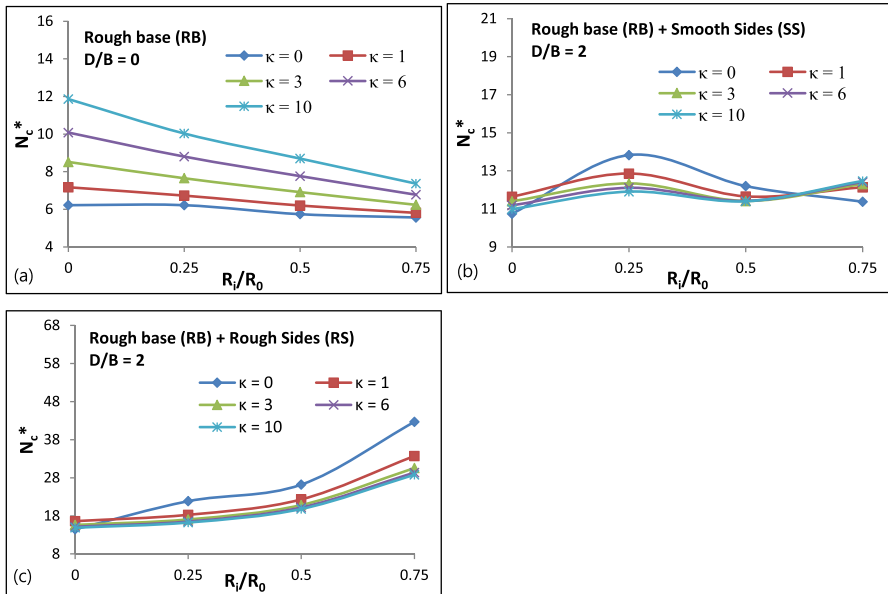


Fig. 9 N_c factor of ring footings for various degrees of non-homogeneity κ , with $D/B=0$ and 2

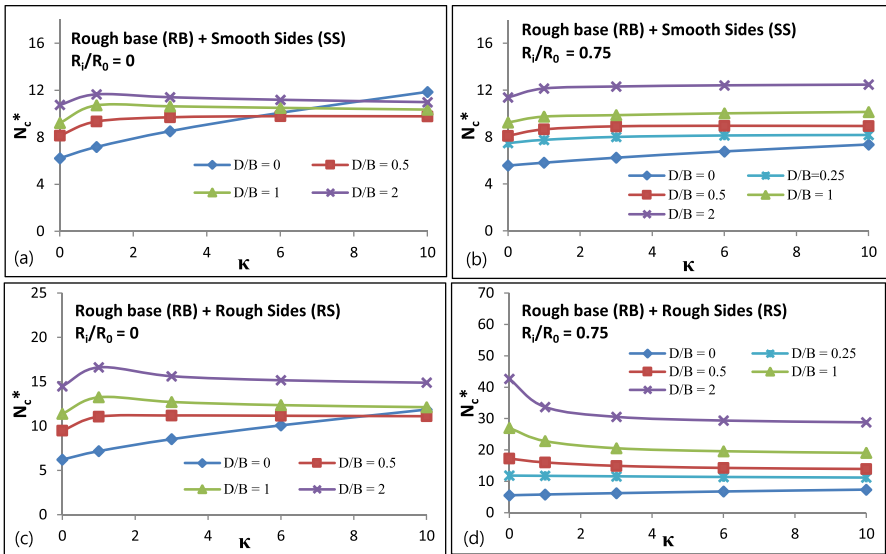
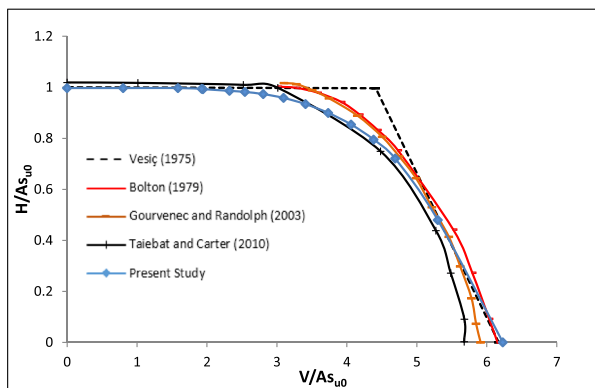


Fig. 10 N_c factor of ring footings for various embedment ratios D/B , with $R_f/R_0=0$ and 0.75

5 Failure envelopes

As shown in Figs. 11–13 for shallow footings in homogeneous soil, the finite difference method is conducted to dress failure envelopes in terms of the dimensionless and normalized loads in two-dimensional loading plane. The interaction of load components is given in terms of vertical-horizontal loading V-H ($M=0$) and vertical-moment loading V-M ($H=0$).

Fig. 11 Comparison of failure envelopes in V-H loading space, for a circular footing



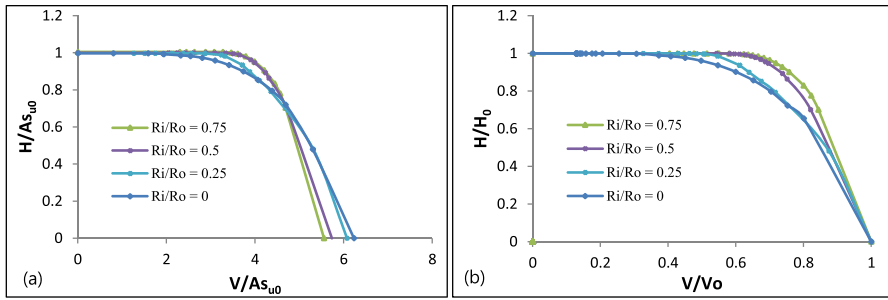


Fig. 12 Failure envelopes in V-H loading space, for ring and circular footings: **a** dimensionless load space, **b** normalized load space

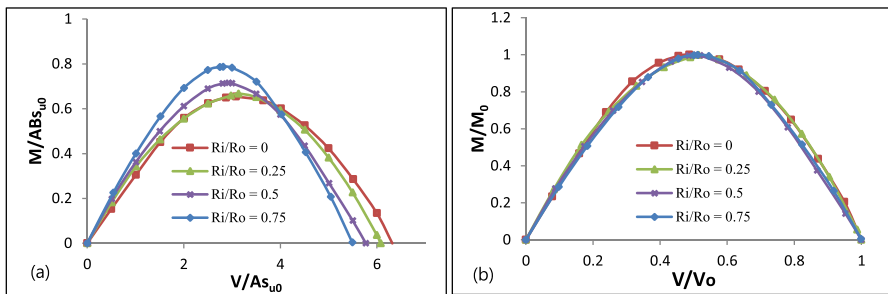


Fig. 13 Failure envelopes in V-M loading space, for ring and circular footings: **a** dimensionless load space, **b** normalized load space

5.1 Combined vertical-horizontal (V-H) loading plan

Figure 11 furnishes a comparison between the current plots of V-H ($M=0$) with those published in the literature. It is noted that the current plot of circular footing is close to that obtained from the finite element analysis conducted by Taiebat and Carter (2010). Subsequently, the size of failure envelope is noticed to be slightly smaller than those predicted by Gourvenec and Randolph (2003) and Bolton (1979).

Figure 12 represents the size of failure envelopes in terms of the combination of vertical and horizontal loads for $R_i/R_0=0, 0.25, 0.5$ and 0.75 . It is noted from Fig. 12a that the size is increasing with the increase of R_i/R_0 for $V/As_{u0} < 5$; however, a decreasing trend is observed for higher vertical loads. In terms of normalized loads (Fig. 12b), it is clear that the shape increases proportionally with the ratio of R_i/R_0 .

5.2 Combined vertical-moment (V-M) loading plane

Figure 13 shows failure envelopes for different R_i/R_0 ratios, with $H=0$ plane. The size of failure envelopes and the maximum moment capacity in Fig. 13a are seen to be increasing with the increase of R_i/R_0 . However, the maximum vertical load drops with the raise of R_i/R_0 . Figure 13b shows that for normalized loads, an almost identical shape of failure envelopes is obtained regardless of the ratio R_i/R_0 .

6 Conclusion

The finite difference code FLAC3D (2006) was employed in order to examine the behavior of ring and circular footings in clay. Elasto-plastic investigations have been conducted for different ring footing geometries, embedment depth ratios D/B , soil heterogeneities κ , and different soil-footing interface conditions. It is important to mention that the current solutions for circular footing have been verified with those available in the literature for the cases of embedded footings and heterogeneous soils.

The results show that the factor N_c depends remarkably on the ratio of inner to outer radius (R_i/R_0), as well as the roughness of the vertical sides. For the case of a homogeneous soil and smooth side interface, N_c relevant to $D/B > 0.25$ decreases with the increase of R_i/R_0 , while for the case of a rough side interface, the increase of R_i/R_0 leads to higher values of N_c . Moreover, the bearing capacity factor relevant to surface footings results in higher values for an increasing trend of κ . For embedded footings, a negligible variation of N_c factors is observed when $\kappa > 3$.

It is of interest to mention that under the vertical-horizontal loading space, both absolute and relative sizes of failure envelopes are observed to be significantly influenced by the ratio R_i/R_0 . Nevertheless, the dimensionless failure load space under vertical-moment loading indicates that the geometry of ring footings (R_i/R_0) reduces the ultimate vertical load capacity and increases the maximum moment capacity, compared to the case of circular footings. Hence, all normalized failure loads in the V-M plane fall into a quite tight band independently of R_i/R_0 .

Author Contribution The basic theme and the methodology of the research were discussed and decided by all authors. All the authors have agreed on the final version of the manuscript.

Declarations

Competing Interests The authors declare no competing interests.

References

- Alzabeebee, S.: Interference of surface and embedded three strip footings in undrained condition. *Transp. Infrastruct. Geotech.* **9**, 250–267 (2022). <https://doi.org/10.1007/s40515-021-00172-9>
- Bolton, M.: *A Guide to Soil Mechanics*. London, MacMillan (1979)

- Boushehrian, J.H., Hataf, N.: Experimental and numerical investigation of the bearing capacity of model circular and ring footings on reinforced sand. *Geotext. Geomembr.* **21**, 241–256 (2003). [https://doi.org/10.1016/S0266-1144\(03\)00029-3](https://doi.org/10.1016/S0266-1144(03)00029-3)
- Eason, G., Shield, R.T.: The plastic indentation of a semi-infinite solid by a perfectly rough circular punch. *Zeitschrift Für Angewandte Mathematik Und Physik ZAMP.* **11**, 33–43 (1960). <https://doi.org/10.1007/BF01591800>
- Edwards, D.H., Zdravkovic, L., Potts, D.M.: Depth factors for undrained bearing capacity. *Géotechnique.* **55**, 755–758 (2005). <https://doi.org/10.1680/geot.2005.55.10.755>
- El Sawwaf, M., Nazir, A.: Behavior of eccentrically loaded small-scale ring footings resting on reinforced layered soil. *J. Geotech. Geo Environ. Eng.* **138**, 376–384 (2012). [https://doi.org/10.1061/\(ASCE\)GT.1943-5606.0000593](https://doi.org/10.1061/(ASCE)GT.1943-5606.0000593)
- Itasca Consulting Group, FLAC3D: Fast Lagrangian Analysis of Continua in 3 Dimensions. Minneapolis, Minnesota, United States, Version 3.1 (2006)
- Gourvenec, S.M., Mana, D.S.K.: Undrained vertical bearing capacity factors for shallow foundations. *Géotechnique Letters.* **1**, 101–108 (2011). <https://doi.org/10.1680/geolett.11.00026>
- Gourvenec, S., Randolph, M.: Effect of strength non-homogeneity on the shape of failure envelopes for combined loading of strip and circular foundations on clay. *Géotechnique.* **53**, 575–586 (2003). <https://doi.org/10.1680/geot.2003.53.6.575>
- Gourvenec, S., Randolph, M., Kingsnorth, O.: Undrained bearing capacity of square and rectangular footings. *Int. J. Geomech.* **6**, 147–157 (2006). [https://doi.org/10.1061/\(ASCE\)1532-3641\(2006\)6:3\(147\)](https://doi.org/10.1061/(ASCE)1532-3641(2006)6:3(147))
- Griffiths, D.V., Fenton, G.A., Manoharan, N.: Undrained bearing capacity of two-strip footings on spatially random soil. *Int. J. Geomech.* **6**, 421–427 (2006). [https://doi.org/10.1061/\(ASCE\)1532-3641\(2006\)6:6\(421\)](https://doi.org/10.1061/(ASCE)1532-3641(2006)6:6(421))
- Hataf, N., Razavi, M.R.: Behavior of ring footing on sand. *Iran. J. Sci. Technol. Trans.* **27**, 47–56 (2003)
- Houlsby, G.T., Wroth, C.P.: Calculation of stresses on shallow penetrometers and footings. *Proceedings of the IUTAM-IUGG symposium on seabed mechanics*, pp. 107–112. Newcastle upon Tyne (1983)
- Hu, Y., Randolph, M.F., Watson, P.G.: Bearing response of skirted foundation on nonhomogeneous soil. *Journal of Geotechnical and Geo Environmental Engineering.* **125**, 924–935 (1999). [https://doi.org/10.1061/\(ASCE\)1090-0241\(1999\)125:11\(924\)](https://doi.org/10.1061/(ASCE)1090-0241(1999)125:11(924))
- Kedar, B., Deepankar, C.: Undrained bearing capacity factor N_c for ring foundations in cohesive soil. *Int. J. Geomech.* **21**, 06020038 (2021). [https://doi.org/10.1061/\(ASCE\)GM.1943-5622.0001900](https://doi.org/10.1061/(ASCE)GM.1943-5622.0001900)
- Kumar, J., Ghosh, P.: Bearing capacity factor N_γ for ring footings using the method of characteristics. *Can. Geotech. J.* **42**, 1474–1484 (2005). <https://doi.org/10.1139/t05-051>
- Lee, J.K., Jeong, S., Lee, S.: Undrained bearing capacity factors for ring footings in heterogeneous soil. *Comput. Geotech.* **75**, 103–111 (2016). <https://doi.org/10.1016/j.compgeo.2016.01.021>
- Mabrouki, A., Benmeddour, D., Mellas, M.: Numerical study of bearing capacity for a circular footing. *Aust. Geomech.* **44**, 91 (2009)
- Mabrouki, A., Benmeddour, D., Frank, R., Mellas, M.: Numerical study of the bearing capacity for two interfering strip footings on sands. *Comput. Geotech.* **37**, 431–439 (2010). <https://doi.org/10.1016/j.compgeo.2009.12.007>
- Martin, C.M.: Vertical bearing capacity of skirted circular foundations on Tresca soil. *Proc. 15th Int. Conf. Soil Mech. Geotech. Engng.* **1**, 743–746 (2001)
- SadeghiFazel, A.H., BolouriBazaz, J.: Behavior of eccentrically inclined loaded ring footings resting on granular soil. *Int. J. Eng.* **33**, 2146–2154 (2020). <https://doi.org/10.5829/ije.2020.33.11b.04>
- Saha, M.C.: Ultimate bearing capacity of ring footings on sand. M. Eng. Thesis, University of Roorkee, Roorkee, UP, India (1978)
- Salgado, R., Lyamin, A.V., Sloan, S.W., Yu, H.S.: Two-and three-dimensional bearing capacity of foundations in clay. *Géotechnique.* **54**, 297–306 (2004). <https://doi.org/10.1680/geot.2004.54.5.297>
- Shu, S., Gao, Y., Wu, Y., Ye, Z.: Undrained bearing capacity of two strip footings on a spatially variable soil with linearly increasing mean strength. *Int. J. Geomech.* **21**, 06020037 (2021). [https://doi.org/10.1061/\(ASCE\)GM.1943-5622.0001904](https://doi.org/10.1061/(ASCE)GM.1943-5622.0001904)
- Taiebat, H.A., Carter, J.P.: A failure surface for circular footings on cohesive soils. *Géotechnique.* **60**, 265–273 (2010). <https://doi.org/10.1680/geot.7.00062>
- Vesic, A. S.: Bearing capacity of shallow foundations. In: Winterkorn, H., Fang, H. Y (eds.) *Foundation engineering handbook*, pp. 121–147. Van Nostrand Reinhold, New York (1975)
- Zhao, L., Wang, J.H.: Vertical bearing capacity for ring footings. *Comput. Geotech.* **35**, 292–304 (2008). <https://doi.org/10.1016/j.compgeo.2007.05.005>

Authors and Affiliations

Skander Hamlaoui¹  · Abdelhamid Messameh² · Abdelhak Mabrouki¹ · Imene Bougouffa¹ · Alaoua Bouaicha¹

Abdelhamid Messameh
ah_messameh@yahoo.fr

Abdelhak Mabrouki
mabroukii@yahoo.fr

Imene Bougouffa
bougouffa-imene@hotmail.com

Alaoua Bouaicha
bouaicha.allaoua@gmail.com

- ¹ Department of Civil and Hydraulic Engineering, LRGC Laboratory, Biskra University, Biskra, Algeria
- ² Department of Civil and Hydraulic Engineering, LARHYSS Laboratory, Biskra University, Biskra, Algeria